Labrador Sea sub-surface density as a precursor of multi-decadal variability in the North Atlantic: a multi-model study

Pablo Ortega[1,2], Jon I. Robson[1], Matthew Menary[3], Rowan T. Sutton[1], Adam Blaker[4], Agathe Germe[4],
Jöel J.-M. Hirschi[4], Bablu Sinha[4], Leon Hermanson[5,] and Stephen Yeager[6]

[1]NCAS, University of Reading, Reading, UK

[2]Barcelona Supercomputing Center, Barcelona, Spain

[3]LOCEAN, Sorbonne Universités

[4]National Oceanography Centre, European Way, Southampton, SO14 3ZH, UK

[5]Met Office Hadley Centre, Exeter, UK

[6]National Center for Atmospheric Research, Boulder, USA

Correspondence to: Pablo Ortega (pablo.ortega@bsc.es)

Abstract. The Subpolar North Atlantic (SPNA) is a region with prominent decadal variability that has experienced remarkable warming and cooling trends in the last few decades. These observed trends have been preceded by slow-paced increases and decreases in the Labrador Sea density (LSD), which are thought to be a precursor of large scale ocean circulation changes. This article analyses the inter-relationships between the LSD and the wider North Atlantic across an ensemble of coupled climate model simulations. In particular, it analyses the link between subsurface density and the deep boundary density, the Atlantic Meridional Overturning Circulation (AMOC), the Subpolar Gyre (SPG) circulation, and the upper ocean temperature in the eastern SPNA.

All simulations exhibit considerable multidecadal variability in the LSD and the ocean circulation indices, which are found to be interrelated. LSD is strongly linked with the strength of subpolar AMOC and gyre circulation, and is also linked with the subtropical AMOC, although the strength of this relationship is   model dependent. The connectivity of LSD with the subtropics is found to be sensitive to different model features, including: the mean density stratification in the Labrador Sea; the strength and depth of the AMOC; and the depth at which the LSD propagates southward along the western boundary. Several of these quantities can also be computed from observations, and comparison with these observation-based quantities suggests that models representing a weaker link with the subtropical AMOC may be more realistic. This would imply that RAPID AMOC measurements might not be adequate to represent decadal to multidecadal changes in the subpolar overturning circulation.

1.   Introduction

The North Atlantic Ocean is a key component in Earth's climate through, for example, its role in redistributing heat and in taking up excess heat and carbon from the atmosphere. It is also a region that has varied significantly in the past. This is particularly true for the North Atlantic subpolar gyre, that has varied significantly on multi-decadal timescales across a range of different variables (Häkkinen and Rhines, 2004; Holliday et al., 2020; Reverdin, 2010; Robson et al., 2018b). Basin-mean sea surface temperature (SST) over the North Atlantic has also been observed to vary on multi-decadal timescales (Schlesinger and Ramankutty, 1994), and has been linked to a range of important climate impacts, including hurricane numbers and rainfall

in monsoon regions (Knight et al., 2006; Monerie et al., 2019; Zhang and Delworth, 2006). The North Atlantic is also expected to change significantly in the future due to the effects of climate change, and consequently produce substantial climate impacts on the surrounding regions (Sutton and Hodson, 2005; Woollings et al., 2012). On decadal timescales, it is the

40 interaction between natural variability and externally forced changes that will shape how the Atlantic regions climate will evolve. Therefore, in order to improve predictions of the North Atlantic, it is imperative that we improve our understanding of the processes that control decadal timescale changes in this region.

It has generally been thought that changes in the ocean circulation, and particularly the Atlantic Meridional Overturning

45 Circulation (AMOC), have played a significant role in shaping multi-decadal variability across the North Atlantic (Knight et al. 2005). In particular, changes in the strength of the AMOC, and its related ocean heat transports have been shown to control multi-decadal internal variability in a range of coupled climate models (Danabasoglu, 2008; Dong and Sutton, 2005; Jungclaus et al., 2005; Ortega et al., 2011, 2015). Changes in AMOC and the wider ocean circulation have been used to explain the changes observed in the subpolar North Atlantic (SPNA), on decadal and longer timescales (Moat et al., 2019). In particular,

50 the SPNA underwent a rapid warming and salinification in the mid 1990s before a decadal timescale cooling and freshening started in 2005, which is consistent with decadal-to-multidecadal variability of the AMOC (Robson et al., 2012, 2013, 2016). The recent cooling has been linked to climate impacts over the continents, including heat waves (Duchez et al., 2016), through an effect on the position on the jet stream (Josey et al., 2018). A long term relative cooling of the SPNA since ~1850 has also been attributed to a centennial weakening of the AMOC (Caesar et al., 2018; Rahmstorf et al., 2015), an AMOC reduction that

55 most CMIP6 model projections predict to continue in the future (Weijer et al., 2020). However, a lack of direct observations of the strength of the AMOC or the ocean circulation more generally have hindered our ability to make a direct attribution of recent changes.

In order to understand the aforementioned changes in the SPNA on multi-decadal timescales many authors have turned to

60 indirect measurements of the AMOC. One particular proxy of AMOC strength that has received some focus recently are density anomalies at depth in the western SPNA or Labrador Sea region. In climate models, density anomalies in the western SPNA are a key predictor of density anomalies further south on the western boundary, and hence of the AMOC strength via thermal wind balance (Hodson and Sutton, 2012; Ortega et al., 2017; Robson et al., 2014, 2016). Observations show considerable decadal variability in subsurface density anomalies; density anomalies in the western SPNA or Labrador Sea

65 between ~1000-2500 m increased significantly and peaked in ~1995 and subsequently declined (Robson et al., 2016; Yashayaev and Loder, 2016). Therefore, these density anomalies have been interpreted as indicating that the AMOC peaked circa mid-to-late 1990s, and then declined, consistent with the warming and then cooling of the eastern SPNA (Hermanson et al., 2014; Ortega et al., 2017; Robson et al., 2016). Time series of subsurface density anomalies in the western SPNA are also consistent with other proxies of AMOC strength including, sea level based proxies (McCarthy et al., 2015; Sutton et al., 2018),

70 sediment based proxies (Thornalley et al., 2018), and upper ocean heat content fingerprints (Caesar et al., 2018; Zhang, 2008). Furthermore, the decline in AMOC suggested by the above proxies is also consistent with the observed AMOC decline at 26°N since 2004 (Smeed et al., 2018), and also with the changes in AMOC seen in ocean data assimilation systems (Jackson et al., 2016, 2019). Therefore, there is confidence that large scale changes in North Atlantic Ocean circulation have occured over the past few decades, and that they have had a significant impact on upper ocean heat content.

75

Although there is consistency across proxies of AMOC changes in the North Atlantic, there are considerable gaps in our understanding and major uncertainties to overcome. For example, the development of the subsurface density proxies has been investigated so far in just a few models (Ortega et al., 2017; Robson et al., 2014). However, there is considerable spread across climate models in the simulations of AMOC mean state and variability (Reintges et al., 2017; Zhang and Wang, 2013), and also in the latitudinal coherence of AMOC anomalies (Li et al., 2019; Roberts et al., 2020; Hirschi et al., 2020), which might reflect different roles of deep density anomalies in the western SPNA on the AMOC, as well as different interplays between the subpolar and subtropical gyre contributions (Zou et al., 2020). Models also do not resolve realistically many key features of AMOC, most notably the overflows, and this affects the subsurface stratification downstream and on the western boundary (Zhang et al., 2011). There also remains significant uncertainty for other important processes. For example, it is not yet clear whether the recent changes in the SPNA are an ocean response to buoyancy forcing, or whether mechanical wind forcing has shaped the recent observed changes (Robson et al, 2016; Piecuch et al. 2017). Local surface fluxes are also likely to explain a significant proportion of the recent cooling (Josey et al, 2018). Subsurface density anomalies are not just a proxy for the AMOC, but more generally for buoyancy forced (or thermohaline) circulation changes, including gyre changes (Ortega et al., 2017; Yeager, 2015). Finally, the AMOC variability is also thought to respond to local wind forcing on a range of timescales, especially at lower latitudes (Polo et al., 2014; Zhao and Johns, 2014), which could disrupt or "mask" the influence of subsurface density anomalies as they propagate further south.

There is also considerable uncertainty in how and where subsurface density anomalies are formed in the SPNA, and how they are related to the AMOC. In observations and models, most water transformation associated with the AMOC occurs within the SPNA, and particularly in the eastern SPNA (Desbruyères et al., 2019; Grist et al., 2014; Langehaug et al., 2012). However, subsurface density anomalies in the western SPNA on decadal timescales have often been linked with buoyancy forcing and changes in deep convection in the Labrador Sea or with changes in the volume of Labrador Sea Water production (Yashayaev and Loder, 2016; Yeager and Danabasoglu, 2014). Many studies have also reported that the basin-wide AMOC in ocean-only and coupled models is sensitive to heat flux or buoyancy forcing in the Labrador Sea (Kim et al., 2019; Ortega et al., 2011, 2017; Xu et al., 2019; Yeager and Danabasoglu, 2014). However, the link between deep convection, deep water formation, and density anomalies at depth in the Labrador Sea is complex, and not fully understood (Katsman et al., 2018). Observations suggest that very little water transformation and deep water formation actually occurs in the Labrador Sea (Pickart and Spall 2007; Lozier et al. 2019). Indeed, recently it has been shown that the Labrador Sea (i.e. OSNAP-west) played very little role in the interannual variability so far observed across the whole OSNAP line (Lozier et al., 2019). Moreover, ocean-only models appear to significantly overestimate the amount of deep water formed within the Labrador Sea, with likely implications for coupled models (Li et al., 2019). These inconsistencies raise the question of whether models are simulating the right relationships.

In this study we will address some of the above uncertainties by performing a multi-model analysis of the North Atlantic in coupled climate models. We focus on the question of how robust is the relationship between subsurface Labrador Sea density anomalies and the basin-wide Atlantic Ocean circulation on decadal timescales. We also assess the question of whether Labrador Sea density can robustly induce density changes over the western continental slope and generate a geostrophic response in the meridional circulation (Bingham and Hughes, 2009; Roussenov et al., 2008). Shedding new light on these links is important for, among other reasons, determining to what extent the RAPID measurements represent the variability of

the basin-wide AMOC cell, as well as to identify the models that can produce more reliable predictions and projections of the SPNA. For this, we will assess specifically the connection between subsurface density and AMOC at high and low latitudes via the western boundary. Furthermore, we will determine whether models consistently support an impact of AMOC changes on the SPNA upper ocean temperatures, and if not, investigate why. Our primary aim is to provide, for the first time in a multi-model context, a broad characterization of these relationships using consistent analysis frameworks and tools, and to document the uncertainty. The reasons for the uncertainty in the relationships will also be explored, establishing links with key model climatological properties that could eventually be exploited as emergent constraints. We intentionally do not explore in detail how subsurface density anomalies are formed in these models, and leave this for further study.

The paper is organised as follows. Section 2 describes the experiments and methods. Labrador Sea density, and its link with the ocean circulation and the wider North Atlantic are explored across the multi-model ensemble in Section 3. The characteristics of the intermodel spread in the previous relationships are explored in Section 4, and Section 5 presents the main conclusions of this study and discusses its implications.

2. Experiments and methods

Here we provide an overview and brief description of the models used in this study and provide some statistical considerations for the intermodel comparison.

2.1. Experiment selection

For the multimodel analysis, we use the preindustrial control simulations (picontrol) from the fifth phase of the Coupled Model Intercomparison Project (CMIP5; Taylor et al. 2012). In particular, we only use those models in which 3D fields of ocean temperature and salinity, as well as the streamfunctions of meridional overturning circulation and/or the barotropic circulation, were available. Twenty different models meet this condition, and their main characteristics have been summarized in Table 1. Most of the models have a nominal horizontal resolution in the ocean close to 1°, and, therefore, cannot resolve the effects of eddies. Menary et al. (2015) has shown for these same model simulations that the effective horizontal resolution can be higher over the Labrador Sea, due to the non-regular grids. Effective resolutions over the area range from 0.47° in the MPI model to 1.6° in IPSL, with these differences determining to a large extent the mean state model biases and the dominant drivers (i.e. salinity or temperature) of the Labrador Sea density changes.

Complementing these simulations, we also consider two control experiments with eddy-permitting resolutions. Specifically, we use a present day control simulation of the HiGEM model, with nominal horizontal resolution in the ocean of 1/3°, and of 0.83° latitude × 1.25° longitude in the atmosphere (Shaffrey et al., 2009), and a pre-industrial control of HadGEM3-GC2 (hereafter, GC2; Ortega et al. 2017) with a nominal resolution in the ocean of 1/4° (ORCA025) and N216 in the atmosphere (i.e. approximately 60 km in the mid-latitudes). The GC2 simulation is the same one employed for the previous analyses of Labrador Sea variability in Robson et al. (2016) and Ortega et al. (2017). Note that we will assume that the present day control in HiGEM can be compared with the other preindustrial simulations due to the large uncertainty these later show in their climatological biases, and so, for the sake of simplicity, we will only refer to preindustrial control experiments from now on. Figure 1 demonstrates that this assumption is reasonable, since the mean Labrador Sea stratification in HiGEM is very similar to that in the other models.

155   As an observationally-constrained reference, this study also includes the assimilation run from DePreSys3, a decadal
prediction system from the MetOffice based on GC2 (Dunstone et al., 2016). In the ocean, the assimilation is performed
through a strong nudging (ten-day relaxation timescale) towards the full fields of a three-dimensional objective temperature
and salinity analysis (Smith and Murphy, 2007). Since it covers a comparatively shorter period (1960-2013), and therefore
different timescales than the control experiments, its comparison with the other simulations will be done with caution, in

160   particular regarding the indices of the large-scale Atlantic circulation, for which other assimilation products show important
discrepancies (Karspeck et al., 2015), thus highlighting significant uncertainty.

Table 1: List of the models used for this study, their characteristics and those of their picontrol simulations. For further details
on the CMIP5 model configurations and components please refer to Table 9.A.1 in Flato et al (2013) and references therein.

Model ID	Lon x Lat ocean resolution (number of vertical levels)	Length	Key variables available
HadGEM3-GC2	1/4° x 1/4° (75 levels)	311 years	AMOC, SPGSI, LSD, NOHT
HiGEM	1/3° x 1/3° (40 levels)	341 years	AMOC, SPGSI, LSD, NOHT
ACCESS1-0	1° x 1° enhanced near Equator and high latitudes (50 levels)	500 years	SPGSI, LSD, NOHT
ACCESS1-3	1° x 1° enhanced near Equator and high latitudes (50 levels)	500 years	SPGSI, LSD, NOHT
CCSM4	1.125° x 0.27–0.64° (60 levels)	1051 years	AMOC, SPGSI, LSD
CESM1-BGC	1.125° x 0.27–0.64° (60 levels)	500 years	AMOC, LSD
CESM1-CAM5	1.125° x 0.27–0.64° (60 levels)	319 years	AMOC, LSD
CESM1-FASTCHEM	1.125° x 0.27–0.64° (60 levels)	222 years	AMOC, LSD
CESM1-WACCM	1.125° x 0.27–0.64° (60 levels)	200 years	AMOC, LSD
CNRM-CM5	0.7° x 0.7° (42 levels)	850 years	AMOC, SPGSI, LSD
CanESM2	1.4° x 0.93° (40 levels)	996 years	AMOC, SPGSI, LSD
FGOALS-g2	1° × 1° with 0.5° meridional in the tropical region (30 levels)	700 years	AMOC, LSD
FGOALS-s2	1° × 1° with 0.5° meridional in the tropical region (30 levels)	501 years	SPGSI, LSD, NOHT
GFDL-ESM2G	1° × 0.85° (63 levels)	500 years	SPGSI, LSD
GISS-E2-R	1.25° x 1° (32 levels)	550 years	AMOC, LSD
GISS-E2-R-CC	1.25° x 1° (32 levels)	251 years	AMOC, LSD
MPI-ESM-LR	1.5° x 1.5° (40 levels)	1000 years	AMOC, SPGSI, LSD
MPI-ESM-MR	0.4° x 0.4° (40 levels)	1000 years	AMOC, SPGSI, LSD

MPI-ESM-P	1.5° x 1.5° (40 levels)	1156 years	AMOC, SPGSI, LSD
MRI-CGCM3	1° × 0.5° (51 levels)	500 years	AMOC, LSD, NOHT
NorESM1-M	1.125° x 1.125° (53 levels)	501 years	AMOC, SPGSI, LSD, NOHT
NorESM1-ME	1.125° x 1.125° (53 levels)	252 years	AMOC, SPGSI, LSD, NOHT

165

2.2.   Methodological considerations

Density values are computed from 3D salinity and potential temperature fields, using the International Equation of State of seawater (EOS-80), and are referred to the level of 2000 dbar (σ_2), to give a stronger emphasis to the deep water properties.

170   Statistical significance of correlation coefficients is assessed following a two-tailed Student's t-test that takes into account the series' autocorrelation to correct the sample size, reducing the degrees of freedom of a series to its effective value (Bretherton et al., 1999).

Because our goal is to provide further insight into the suggested relationships established from observed trends in the North Atlantic (e.g., Robson et al., 2016), all statistical analyses in this study exploring the relationships between variables and
175   associated lags are based on 10-year running trends. This is analogous to the calculation of a typical 10-year running mean, but computing over each 10 year period a linear trend instead and keeping the slope value. Note also that our main results remain similar if decadal running means are applied instead (not shown), as both are alternative approaches to concentrate on the low-frequency variability. Running trends have also the particular advantage of not being sensitive to long-term drifts, which are still present (and can be important for some simulations and variables) when running means are computed. To illustrate how
180   decadal running trends represent low-frequency variability, these have been included in Figure 2b for an index of Labrador Sea density.

3.   Labrador Sea density as an index of multi-decadal North Atlantic variability

This section explores the potential of Labrador Sea density as a proxy of the ocean circulation changes in the North Atlantic. As in our previous studies (Ortega et al., 2017; Robson et al., 2016), the indices that we will herein define represent waters
185   within the Labrador Sea and not those that are necessarily formed in the region (e.g. Labrador Sea Water). Since Labrador Sea variability is affected by different processes (e.g. vertical mixing, Arctic-Atlantic overflows, sea ice interactions) that can be represented differently in the models, both in time and space, we characterize its variability over a relatively broad box (60°W-35°W; 50°N-65°N, blue box Figure 1a) that also includes part of the Irminger Sea region. Note that over this large area EN4 (Good et al., 2013), an objective analysis of monthly temperature and salinity 3D observations, shows the weakest density
190   stratification in the North Atlantic (characterised in Figure 1a as the density difference between 1000m and the surface).

3.1.   Labrador Sea density across models

A first indicator of potential model discrepancies is Labrador Sea stratification, which can lead to differences in the representation of deep ocean convection (i.e. weaker density stratifications will facilitate the mixing, fostering convection activity, and vice versa for stronger density stratifications). Figure 1b-d illustrates the inter-model differences with the vertical
195   profile of the spatially averaged Labrador Sea temperature, salinity and density. The largest discrepancies are seen for

temperature. Most models present their warmest waters at the surface, and temperatures decrease sharply to minimum values around 100 m and increase again at deeper levels, reaching uniform conditions after approx 300 m. However, the location and magnitude of this temperature minimum and the two maxima are highly variable. It is important to note that the profile for one of the models, MRI-CGCM3, is noticeably different to the others, with a subsurface minimum more than 2 degrees colder

200 than for any of the other models. In terms of salinity, the general profile is more coherent across models, with minimum salinity at the surface that progressively increases with depth and attains uniform values after 500 m. Density stratification seems to be determined by salinity, as their two vertical profiles show similar features. This similarity includes exceptionally strong density and salinity stratification in MRI-CGCM3 as compared with the other models. This stratification is so strong that it precludes the occurrence of deep convection (not shown). Because of this, MRI-CGCM3 is an outlier for many of the

205 metrics used in the paper, and has been excluded for the subsequent analyses to facilitate the interpretation of our results. We also note that the profiles for the two eddy-permitting models (green and orange lines in Figure 1b,d) lie within the spread of the CMIP5 models, indicating that resolution (at least to eddy-permitting spatial scales) does not drastically change stratification in the region. The DePreSys3 assimilation run closely matches the stratification in EN4, which supports DePreSys assimilation run as a reasonable observation-constrained reference for the models. The comparison of both

210 observation-based datasets with the rest of simulations suggests that, in the subsurface, all models are too warm and most of them are too salty, two biases that have a competing effect on the mean subsurface density. Because of these canceling effects, several models show a good representation of the subsurface densities when compared to EN4 and DePreSys3. This compensation of model shortcomings for temperature and salinity is clearly illustrated in HiGEM, which shows a remarkable agreement with EN4 below 500 m.

215 To represent the characteristic interannual variability of Labrador Sea densities (hereafter referred to as LSD for consistency with previous work), we perform an Empirical Orthogonal Function (EOF) analysis and extract the leading mode for the annual means of LSD (Figure 2a), as in Ortega et al. (2017). For all simulations the first EOF of LSD exhibits a vertical structure where density values are largest at or near the surface and gradually decrease with depth. Thus, this first EOF typically reflects situations in which the climatological vertical profile in Figure 1 is weakened or strengthened, depending on

220 the sign of the corresponding principal component. Some inter-model discrepancies are evident, in particular regarding the depths where the maximum density values are found, which can happen between the surface and 500 m. Despite these differences, the dominant timescales of LSD variability seem to coincide between models. For example, Figure 2b illustrates the first principal component of LSD (PC1-LSD) for GC2 and HiGEM, showing in both cases important multidecadal variability. Furthermore, Figure 2c shows the Fourier spectrum analysis of the annual PC1-LSD values, and most models show

225 enhanced PC1-LSD variability for periodicities between 5 and 30 years.

It is worth noting that the PC1-LSD index used here is different to the deep LSD index introduced in Robson et al (2016). The deep LSD index is defined as the 1000-2500 m vertical mean of the spatially averaged density over the same region as PC1-LSD. We now compare how both indices represent the low-frequency changes in LSD, described in this paper as decadal running trends. A lead-lag correlation between the decadal trends in both PC1-LSD and deep LSD indices shows that they are

230 strongly correlated in all models. However, some differences emerge when considering the lag of maximum correlation (Figure 2d). This comparison might indicate, once again, that decadal variability of subsurface density is concentrated at different depths in different models. It is also possible that both indices are sensitive to changes in deep water formation in different locations (e.g. Irminger or GIN Seas), which could, hence, affect the depth and maximum lag of the correlations.

Nevertheless, we adopt PC1-LSD for the rest of the analyses, as it has the advantage of adjusting in each model to the depths

235   in which density variability is more prominent.
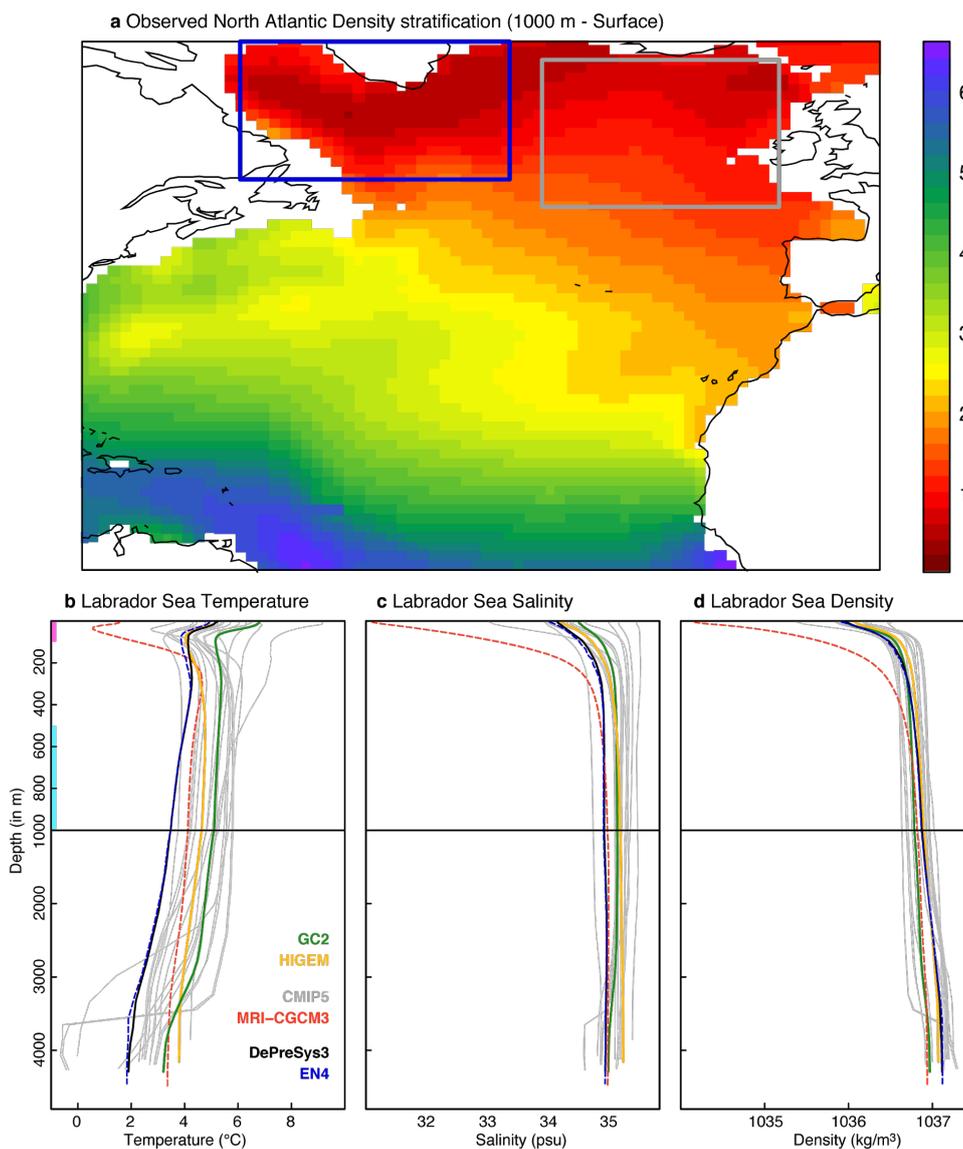
Figure 1: a Climatological difference between subsurface (1000m) and surface density (2) in the North Atlantic in the observational dataset EN4 (Good et al., 2013). The reference period to compute the climatology is 1960-2013. The grey box (32°W-10°W and 47°N-63°N) encloses the region where the ESPNA-T700 index in Figure 4d is computed. **b-d**

240   Climatological mean of the spatially averaged Labrador Sea (60–35°W, 50–65°N, blue box in panel *a*) temperature, salinity and density as a function of depth in the simulation ensemble, the DePreSys3 assimilation run and EN4. The magenta (cyan) bars in the vertical axis correspond to the depths that have been used to define the vertical stratification Labrador Sea indices. For each model and dataset the climatology is computed for its whole length except for EN4, that is computed for the overlap period with the DePreSys3 assimilation run.
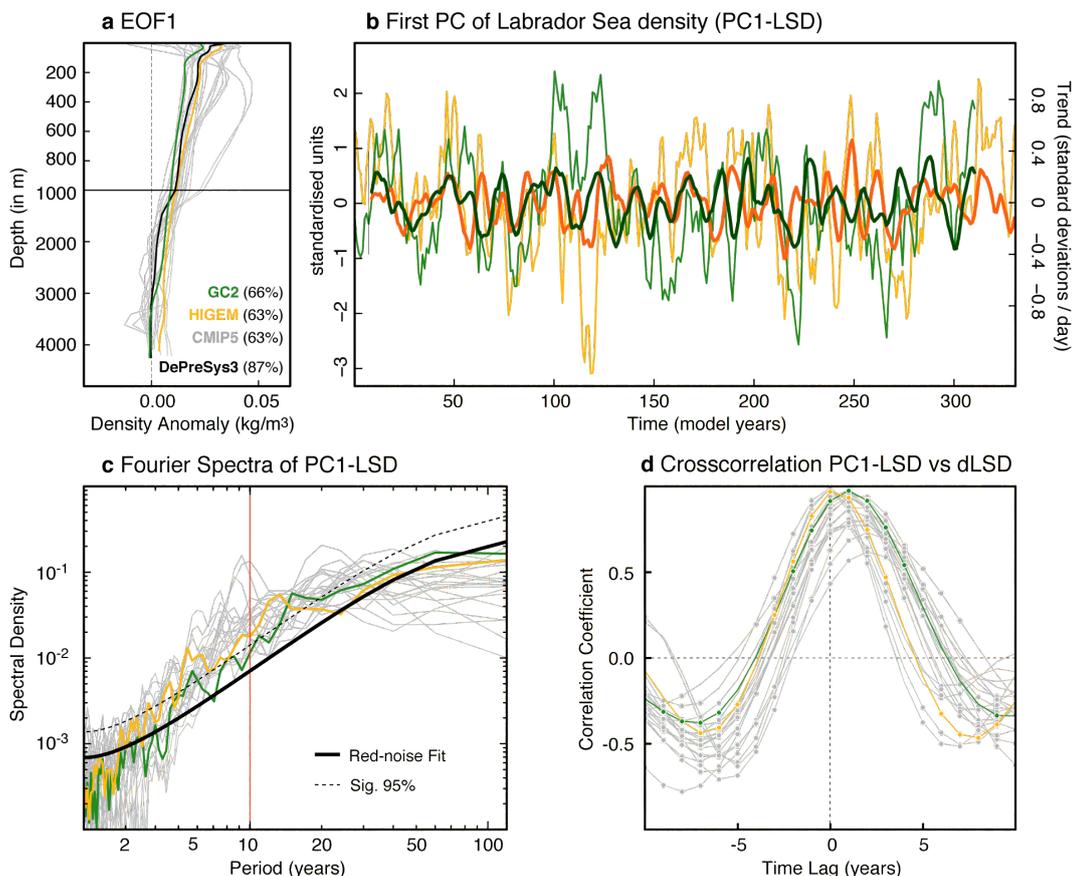
Figure 2: a First empirical orthogonal function (EOF) as a function of depth of the spatially averaged LSD in all the preindustrial experiments and in the DePreSys3 assimilation run. The percentage of variance explained by this mode in each model is included in brackets in the legend (for the CMIP5 runs, this represents the mean value across the ensemble). **b** Associated principal component of the spatially averaged LSD (PC1-LSD) in the two high-resolution experiments. Thin lines represent the raw yearly-resolved PC1-LSD timeseries, while thick lines represent their associated 10-year running trends centered around the last year of the decade over which the trend is computed. **c** Normalized Fourier spectra of the PC1-LSD index in each of the preindustrial simulations. The black thick line represents a red noise process with the same first autoregressive (AR1) coefficient as PC1-LSD in GC2, and the dashed line sets the 95% confidence interval of this red-noise process. No major differences are found when using HiGEM's AR1 coefficient instead. The red vertical line highlights the 10 year periodicity. **d** Lead-lag correlations between the decadal trends in PC1-LSD, and those in the deep LSD index from Robson et al. (2016), defined as the 1,000–2,500 m average density in the box 60–35°W, 50–65°N. Positive lags indicate that PC1-LSD leads the changes in deep LSD. Full dots denote correlation values exceeding a 95% confidence level based on a student's t-test that takes into account the series autocorrelation.

3.2.   Labrador Sea density linkages with the ocean circulation

The link between PC1-LSD and other ocean circulation indices in the North Atlantic is now examined. Three indices are considered: the AMOC at two different latitudes, 26°N (i.e. the same latitude as the RAPID array) and 45°N to capture the typical variability of the subpolar AMOC, and an index of the subpolar gyre strength. The AMOC indices are computed as the

maximum of the North Atlantic overturning circulation at any depth. Furthermore, the Ekman component is removed to focus
on the slow wind-forced and the thermohaline-driven (i.e. the only one that can be influenced by the PC1-LSD directly)
265   AMOC changes. To compute the Ekman component, we vertically integrate the Ekman velocities (after introducing a depth-
uniform return flow to ensure no net meridional mass transport) following Eq. 6 in Baehr et al. (2004).   This   Ekman
component is then removed at each depth level, prior to the calculation of the AMOC indices. The subpolar gyre strength is
computed as an average of the North Atlantic barotropic streamfunction in the Labrador Sea region (60–35°W, 50–65°N),
where the gyre strength is usually maximum. Since the SPG circulation is cyclonic and, therefore, associated with negative
270   barotropic streamfunction values, the subpolar gyre strength index (SPGSI) is multiplied by -1 so that an intensification of the
gyre corresponds to a positive value of the index. The Fourier spectra of the raw ocean circulation indices (Figure 3) show
that, similar to the PC1-LSD, all three indices have strong multidecadal variability, with the largest differences with respect to
PC1-LSD emerging for the timescales between 10 and 30 years, in which the spectral power is comparatively weaker, in
particular for the AMOC26 index, and at 50 and longer timescales, in which the ocean circulation indices appear to have
275   enhanced variability with respect to PC1-LSD.
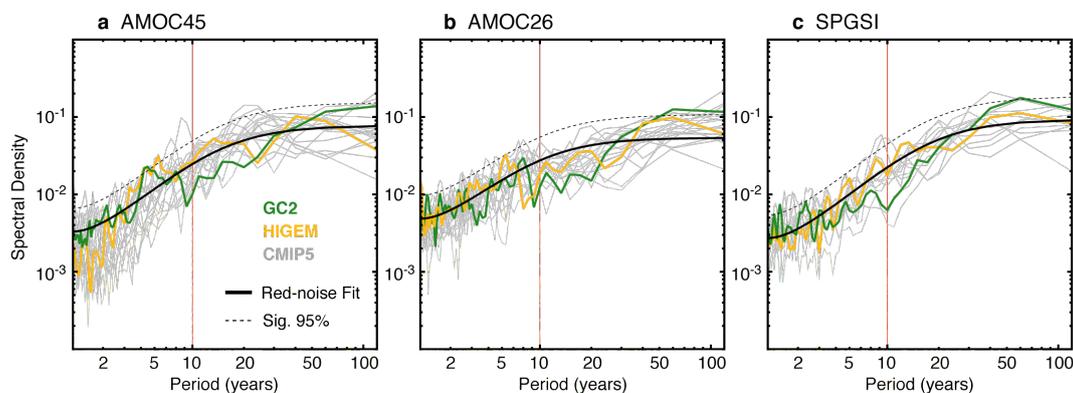
Figure 3: a-c Fourier spectra in the picontrol ensemble for the indices AMOC45N, AMOC26N and SPGSI. Red-noise spectra
corresponding to a 1st order autoregressive process fit to GC2 indices are provided as reference.

280   Figure 4a shows that decadal trends in PC1-LSD are associated with trends in the AMOC at 45°N (AMOC45). Nevertheless,
there is some inter-model spread regarding the lag of maximum correlation, which ranges between 0 and 2 years (with PC1-
LSD leading), although both variables are in phase for the majority of models. The AMOC at 26°N (AMOC26) is also
positively related to PC1-LSD, with PC1-LSD leading AMOC26 by three years on average (Figure 4b). However, the average
correlation between PC1-LSD and AMOC26 is weaker, and the spread in the magnitude and lag of the maximum correlation
285   is larger than for AMOC45. Therefore, it appears that the link with the subtropics is weaker than for 45°N and that AMOC
coherence between subpolar latitudes and the subtropics in coupled models is model dependent. The reasons for the spread in
the relationship between PC1-LSD and AMOC26 are explored in Section 4. A strong relationship is also found between PC1-
LSD trends and those in SPGSI (Figure 4c), of similar order than for AMOC45. Thus, overall, PC1-LSD is a good proxy for

the large-scale ocean circulation in the Subpolar North Atlantic, and can also be a precursor for a fraction of the AMOC

290 variability in the subtropical Atlantic. This result is further supported by a parallel analysis in Figure 5, looking at the

maximum correlation between the decadal AMOC trends and those in Labrador Sea density as a function of depth, when the

latter leads the AMOC by up to 10 years. Figure 5 reveals that the strongest link between the Labrador Sea densities and the

AMOC, both at 45 and 26°N, occurs in its first 1000 m, the same levels where the first EOF of LSD show the maximum

loadings (Figure 2a), which confirms the appropriateness of using PC1-LSD to represent the ocean circulation. The same

295 analysis also supports a strong link between SPGSI and LSD, although in that case the largest correlations usually happen at

deeper levels (between 1000 and 2000 m). Note also that the main conclusions drawn from PC1-LSD are also valid for the

dLSD index: however, the inter-model differences are larger (Supplementary Figure 1).
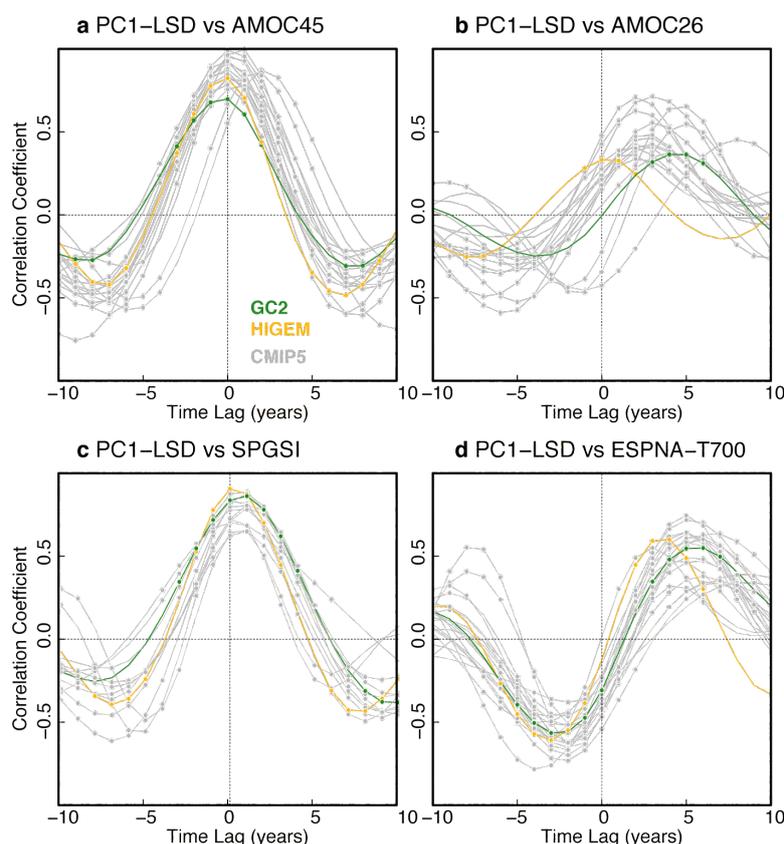
Figure 4: a Lead-lag correlations across the picontrol ensemble between the PC1-LSD index and the maximum AMOC
300 streamfunction at 45°N after the Ekman transport is removed (AMOC45). Correlations are based on 10-year running trends.
Significance is assessed as in Figure 2d and indicated with a circle. For positive lags, PC1-LSD leads. **b-d** The same as in *a*
but between PC1-LSD and the maximum AMOC streamfunction at 26°N after the Ekman transport is removed (AMOC26),
the subpolar gyre strength index (SPGSI) and the vertically averaged top 700 m temperatures in the eastern subpolar gyre
(ESPNA-T700; grey box in Figure 1a).

305
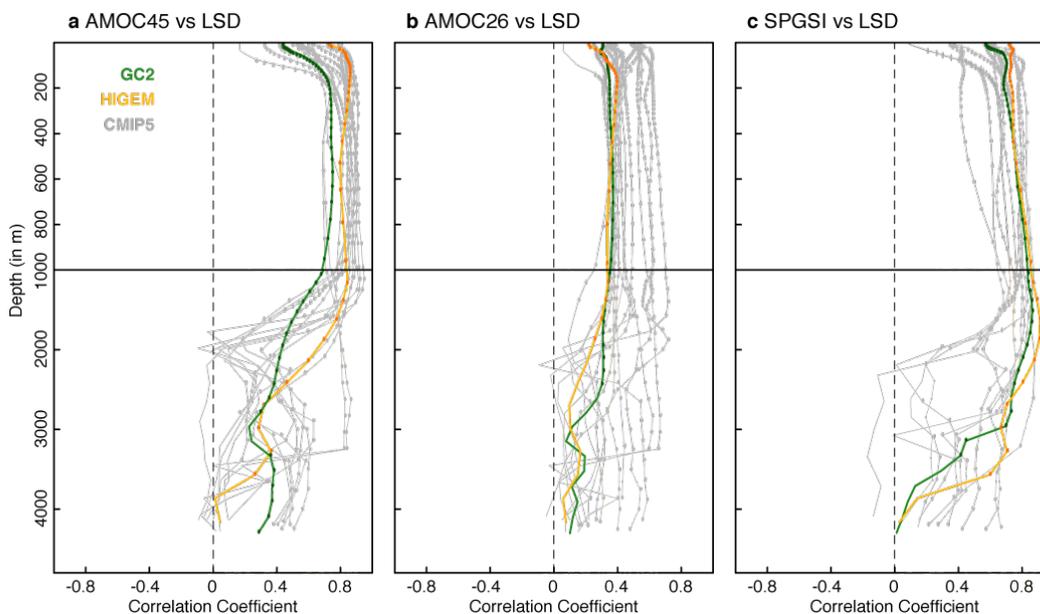
Figure 5: a Maximum correlation (at any lag) between the AMOC45 index (after the Ekman transport is removed) and Labrador Sea Densities as a function of depth for all the simulations. Colored dots indicate correlations that are significant at the 95% confidence level. **b-c** The same as in *a* but between the AMOC26 index and LSD, and between the SPGSI and LSD, respectively.

3.3.   Labrador Sea density linkages with the wider North Atlantic

Previous studies based on the GC2 picontrol simulation have suggested LSD to be also a potential predictor of wide-spread cooling events in the eastern SPNA, like the observed cooling over 2005 to 2015 (Robson et al. 2016; Ortega et al. 2017). We thereby continue our exploration of the PC1-LSD index by investigating its link with the eastern SPNA in the multi-model ensemble. To explore this link we introduce a new index that represents the mean temperature in the eastern SPNA region (32°W-10°W,47°N-63°N) averaged over the top 700 m of the ocean (ESPNA-T700). Lead-lag correlations between the decadal trends in PC1-LSD and this index (Figure 6a) show that there is a coherent relationship between both variables across models, with PC1-LSD increases (decreases) being consistently followed by ESPNA-T700 warmings (coolings). Nevertheless, there are inter-model differences concerning the magnitude and lag of the strongest positive correlations, revealing important uncertainty in the relationship. The spread in the PC1-LSD vs ESPNA-T700 relationship is thus reminiscent of the spread found between PC1-LSD and AMOC26, which suggests that they might be related. We also note significant negative correlations when ESPNA-T700 leads PC1-LSD by 2-4 years that might be explained by the opposed (and nearly concomitant) impacts that the NAO exerts on both variables (Figure 6b,c). Positive NAO phases, and associated surface buoyancy forcing (Lozier et al., 2008) lead in first instance to negative SST (Barrier et al., 2014; Lohmann et al., 2009) and an almost simultaneous cooling in ESPNA-T700 (Figure 6b). In comparison, on the western side of the SPNA, positive NAO phases contribute to reduce vertical density stratification, favoring convection and a more positive LSD index (Robson et al., 2016), which in the models lags the NAO by 2-3 years (Figure 6c). The fact that correlations between NAO and ESPNA-T700 are weaker than between PC1-LSD and ESPNA-T700 suggests that the ocean might also be playing an additional role.
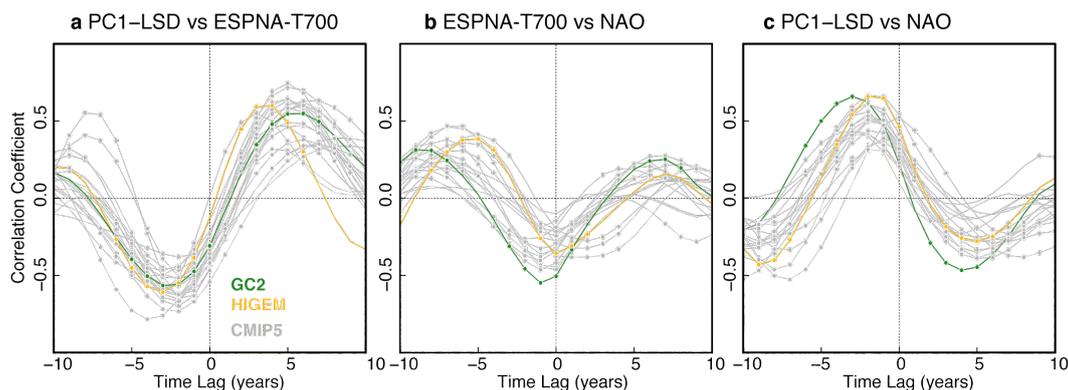
330   **Figure 6: a** Lead-lag correlations across the picontrol ensemble between the PC1-LSD index and the vertically averaged top
700 m temperatures in the eastern subpolar gyre (ESPNA-T700; grey box in Figure 1a). Correlations are based on 10-year
running trends. Significance is assessed as in Figure 2d and indicated with a circle. For positive lags, PC1-LSD leads. **b-c** The
same as in *a* but between the North Atlantic Oscillation (NAO; defined as the standardised difference in sea level pressure
between the closest grid-points to Azores and Reykjavik) and the ESPNA-T700, and between the NAO and the PC1-LSD,
335   respectively. In these two cases, for negative lags the NAO leads.

The link between PC1-LSD and the ESPNA could be explained through an influence of the first on the meridional ocean heat
transport. This link is now investigated in the two eddy-permitting simulations (Figure 7) and in the five CMIP5 models for
which the ocean heat transport fields are publicly available. In the two high resolution experiments and two of the CMIP5 ones
340   the decadal trends in the meridional ocean heat transport at 45°N (OHT45) are strongly linked with those in PC1-LSD. This is
a similar relationship to the one previously found in Figure 4 between PC1-LSD and both the AMOC45 and SPGSI, but in this
case with PC1-LSD leading with slightly longer lead time. The other CMIP5 experiments support a weaker, yet significant,
link, as well as a longer lag between OHT45 and PC1-LSD. Altogether, Figure 7a confirms that PC1-LSD is a good precursor
of the changes in the meridional ocean heat transport, although with some differences across models which might reflect a
345   different representation of certain processes. The contributions of two different processes to this delay are further investigated
in HiGEM, for which OHT had been decomposed online at each time-step into vertical and horizontal heat transports (as in
Bryan, 1969), which can be respectively interpreted as the "overturning" (i.e. characterised by the zonal mean transport) and
"gyre" (i.e. characterised by variations from the zonal mean transport) components (Robson et al., 2018a). While the
overturning contribution ($OHT45_{over}$) increases in phase with the AMOC45, SPGSI and PC1-LSD changes (Figure 7b), the
350   increase in the gyre component (OHC_{gyre}) starts four years later. That could be the time required in HiGEM for the propagation
of mean and/or anomalous temperatures from the southern to the northern branch of the SPG.
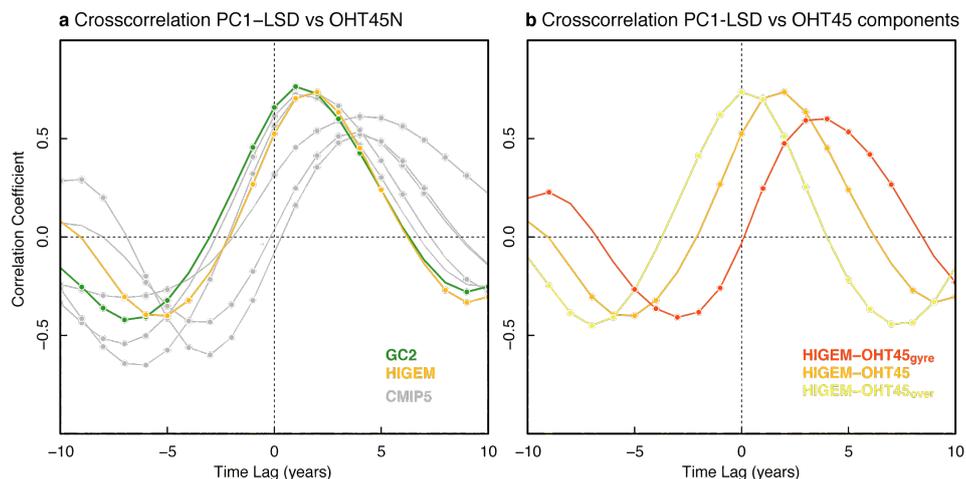
Figure 7: a Lead-lag correlations in a subset of the picontrol experiments between the PC1-LSD index and the ocean heat transport across the 45°N transect (OHT45N). Note that the ocean heat content is only available for 5 models of the CMIP5 ensemble. Correlations are based on 10-year running trends. **b** The same as in *a* but only in HiGEM for the different terms of the OHT45N. For positive lags, PC1-LSD leads.

4.   Characteristics of the inter-model spread in subpolar to subtropical AMOC

This section investigates which particular climatological model features are linked to the large inter-model spread in the PC1-LSD vs AMOC26 relationships. The most relevant model features thus identified will improve our process understanding, and can eventually be used to identify which models are most realistic and, in turn, can deliver more reliable projections of the future changes in the North Atlantic.

Figure 8 shows that models that simulate a stronger and deeper climatological AMOC (both at 45°N and 26°N) tend to have a stronger correlation between PC1-LSD and the subtropics. All these linear relationships between climatological AMOC strength and depth and the PC1-LSD vs AMOC26 connectivity are significant at the 95% confidence level. These climatological AMOC values (without Ekman) can be put in context with those from RAPID observations and DPS3. RAPID observational uncertainties have been considered by including the mean values over three different non-overlapping periods (i.e. 2004-2007, 2008-2012 and 2013-2016; dotted lines in Figure 8). The scatterplots show that the majority of models whose climatological AMOC26 lies within the RAPID/DPS3 climatological spread have a relatively weak link between PC1-LSD and AMOC26, although some models supporting a strong link are also included or remain close to the RAPID/DPS3 values. However, caution is recommended, e.g., before defining emerging constraints, because model and observations are not directly comparable for numerous reasons: both RAPID and DPS3 cover shorter periods than the simulations and relate to different background forcing conditions (present day vs preindustrial) which might imply different mean states (Thornalley et al., 2018). Furthermore, evidence suggests RAPID calculations from mooring arrays might be underestimating the AMOC strength by ~1.5 Sv (Sinha et al., 2018).
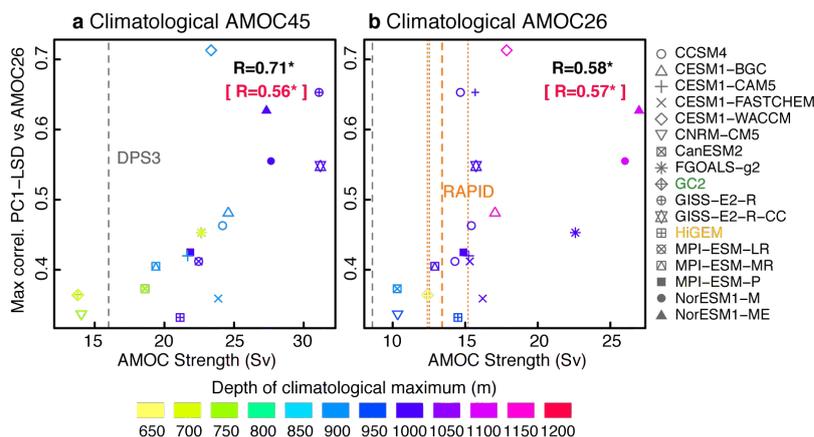
Figure 8: a-b Scatterplot of the maximum correlations at any lag between PC1-LSD and AMOC26N against the climatological AMOC45N and AMOC26N means, respectively. All AMOC indices refer to the values after the Ekman transport signal is removed. The maximum correlations are based on 10-year running trends. Colors indicate the depth at which the climatological AMOC maximum occurs. The correlation coefficient between the maximum PC1-LSD correlation and the climatological mean AMOC is shown in the top-left corner in black. In magenta, the analogous correlation but against the depth of the mean climatological AMOC is shown. The presence of an asterisk indicates that the correlation is significant at the 95% confidence level. The dashed grey vertical lines mark the climatological AMOC strength value in the DePreSys3 assimilation run. The orange vertical lines indicate the climatological value from RAPID observations (Smeed et al., 2018) from 2004 to 2016 (dashed), and in three non-overlapping sub-periods of 4 years (dotted).

A potentially important factor behind the inter-model spread in Figure 4b is the mean density stratification in the Labrador Sea. Figure 9 suggests that, indeed, the PC1-LSD vs AMOC26 spread is partly influenced by the density stratification in this region. Models with a weaker density stratification have a stronger relationship between PC1-LSD and AMOC26. However, no link is found between the PC1-LSD vs AMOC26 relationship and temperature or salinity stratification in the Labrador Sea. Models that have a weaker density stratification (here defined as the difference between the top 100 m, and the average between 500-1000 m), and thus favor deeper convection in the Labrador Sea, generally exhibit a stronger link between PC1-LSD and AMOC26. This result is robust for other stratification indices based on different depth levels (See Supplementary Figure 2). It is also worth mentioning that all models except CanESM2 are more weakly stratified in the Labrador Sea than the observations (represented herein by the DePreSys3 assimilation run and EN4). Hence, the real link of LSD with the AMOC26 may not be as strong as some models suggest.
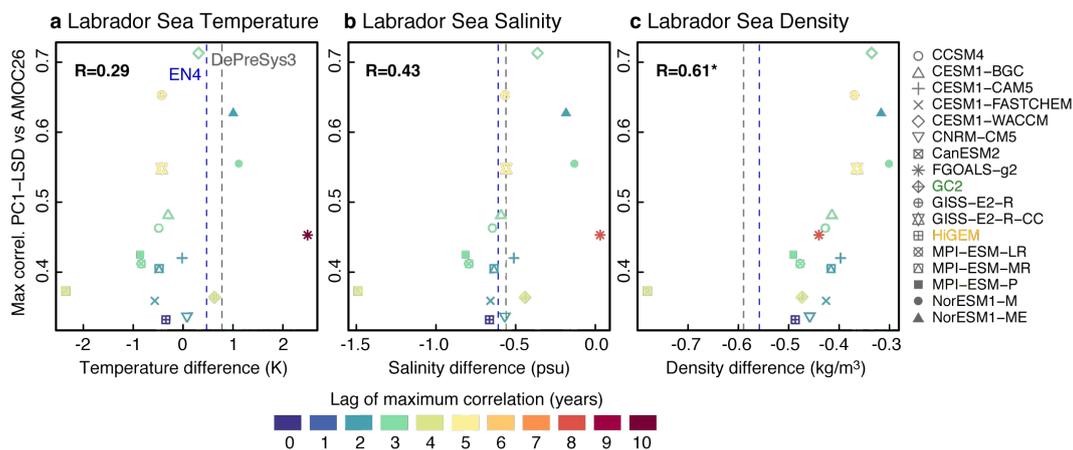
Figure 9: a Scatterplot of the maximum correlations at any lag between PC1-LSD and AMOC26N (without the Ekman component) against the climatological mean of the Labrador Sea temperature stratification index (computed as the difference
400 of the vertical means in the levels 0-100 m minus the vertical means in the levels 500-1000 m; see Fig. 1). The maximum correlations are based on 10-year running trends. The correlation coefficient between the two metrics is shown in the top-left corner. The presence of an asterisk indicates that the correlation is significant at the 95% confidence level. Colors indicate the lag at which the maximum correlation between PC1-LSD and AMOC26 is obtained. The grey (green) vertical lines depict the mean stratification value in the DePreSys3 assimilation run EN4. In both cases, their overlap period is used to compute the
405 climatology (i.e., 1960-2013). **b-c** The same as in *a* but for the Labrador Sea salinity and density, respectively.

Another key aspect of the LSD vs AMOC26 connectivity is the western boundary density. Indeed, boundary density is critical to the mechanism through which LSD influences the AMOC at lower latitudes. Positive (negative) LSD anomalies propagate equatorward following this boundary, and as they do so they strengthen (weaken) the zonal density gradient, triggering a
410 thermal wind response that accelerates (decelerates) the AMOC. In the following we investigate differences in the propagation of boundary densities across models, and if these differences can affect the inter-model PC1-LSD vs AMOC26 spread. Figure 10 focuses on the two high-resolution simulations, where important differences already manifest. It represents the correlations of PC1-LSD with the density fields near the western boundary at four different longitudinal transects: 57°N (cutting across the Labrador Sea), 45°N, 35°N and 26°N. In both models, the depth of the maximum correlation near the continental shelf is
415 coherent across latitudes. However, in HiGEM these occur at deeper levels (1000 to 3000 m) compared to GC2 (1000 to 2000 m), and the difference is especially clear at 35°N, where the highest correlations occur at ~2000 m in HiGEM, while only at 1000 m in GC2. Similar depth differences are also found at 26°N, but with slightly weaker correlations. In addition to the difference in the depth of the maximum correlation between HiGEM and GC2, there are differences in the vertical structure between the two models. For example, at 35°N in GC2, density anomalies on the western boundary form a tripole (low
420 correlation above and below the maximum correlation at ~1000 m), but in HiGEM the density anomalies form a dipole (Figure 10f). We note some differences in bathymetry at this latitude (which is steeper in HiGEM), which might partly explain some of the differences in terms of the density correlation structure.

425
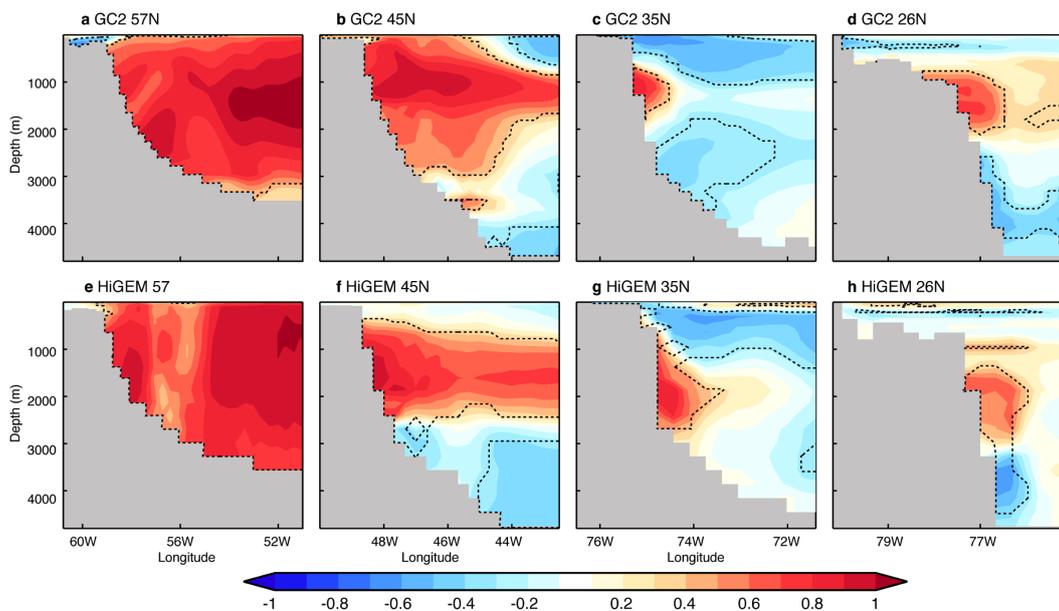
Figure 10: a In-phase correlation in GC2 between the PC1-LSD index and the density fields across a zonal section at 57°N located in the vicinity of the western Atlantic boundary. Thin dashed contours enclose areas where the correlation significance exceeds the 95% confidence level. Correlations are based on 10-year running trends. **b-d** The same as in *a* but for zonal sections at 45°N, 35°N and 26°N. **d-h** The same as in *a-d* but for HiGEM.

430

Figure 11 shows that the diversity in the depth of these boundary densities is even more evident when including the CMIP5 models. The depth of the maximum correlation between PC1-LSD and the western boundary density at the four latitudinal sections relates linearly (and significantly at the 95% confidence level) across models with their PC1-LSD vs AMOC26 correlation. In this case, models exhibiting deeper WBDs generally show stronger links between LSD and the subtropical

435 AMOC. We also checked if models with stronger correlations at the WBDs also support a stronger link between the LSD and the AMOC (correlations in magenta in Figure 11), but this only holds true at 57°N. This suggests that the depth along which WBDs propagate southward, and/or the vertical structure of anomalies, are the key aspects to understand and potentially narrow down the spread.
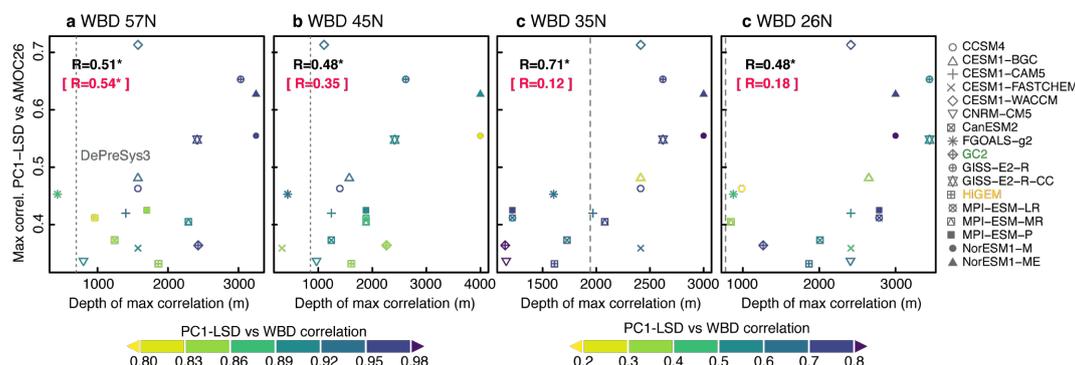
Figure 11: a Scatterplot of the maximum correlations at any lag between PC1-LSD and AMOC26N (without the Ekman component) against the depth at which the maximum correlations at any lag between PC1-LSD and the WBD at 57°N occur. The maximum correlations are based on 10-year running trends. The correlation coefficient between the two metrics is shown in black the top-left corner. Likewise, another correlation coefficient in magenta is shown, computed between the PC1-LSD and AMOC26N maximum correlation and the PC1-LSD and WBD at 57N maximum correlation. The presence of an asterisk indicates that the correlation is significant at the 95% confidence level. Colors indicate the maximum correlation between PC1-LSD and the WBD. The grey vertical lines depict the corresponding depth of maximum correlation for the DePreSys3 assimilation run . **b-d** The same as in *a* but for the WDB at 45, 35 and 26°N, respectively.

5. Conclusions and discussion

This article has explored, in a multi-model context, the linkages between subsurface density in the subpolar North Atlantic (SPNA) and the ocean circulation further south. In particular, it has explored the role of Labrador Sea density (LSD) in driving Western Boundary Density anomalies (WBD) and the ocean circulation, and the impact on upper ocean temperature changes in the SPNA. The analysis was based on two control simulations with eddy-permitting models, a preindustrial one with HadGEM3-GC2 and a present day one with HiGEM, and on 20 CMIP5 preindustrial experiments. Furthermore, where possible these characteristic model features have been computed in observational datasets, as well as in a simulation assimilating observations. The major findings are listed below:

- All the simulations show clear multidecadal variability in Labrador Sea density. There is also a close link between LSD and the strength of the subpolar Atlantic Ocean circulation, with positive density anomalies leading to a strengthening of the Atlantic Meridional Overturning Circulation (AMOC) at 45°N and the Subpolar Gyre (SPG) circulation.
- The relationship between anomalous LSD and the strength of the AMOC at 26°N - the latitude of the RAPID array measurements - is also positive in the simulations, but there are significant inter-model differences, both in the strength of the relationship and the lag of maximum correlation. This uncertainty implies that the connectivity of LSD with the subtropics and latitudinal AMOC coherence is model-dependent.
- The connectivity between anomalies in LSD and AMOC at 26°N is sensitive to different model features, including the strength and depth of the climatological AMOC maximum, the mean density stratification in the Labrador Sea, and the depths at which the LSD propagates southward along the western boundary. Stronger LSD connectivity with the subtropics tends to occur in models with a stronger and deeper AMOC, weaker Labrador Sea stratification and western boundary density propagating at deeper levels.

-   Observationally derived constraints of the model based relationships tend to suggest that the link between LSD and the subtropical AMOC is weak. This suggests that observations of AMOC via RAPID may not be representative of the basin wide buoyancy forced AMOC variability. However, caution is advised because simulations and observations are not directly comparable, and so significant uncertainty remains in constraining the relationship between LSD and subtropical AMOC.

-   The multi-model ensemble does also support a significant lagged relationship between LSD and the upper ocean temperature in the eastern SPNA, in line with previous studies linking LSD to the recently observed changes in the North Atlantic. However, models disagree regarding the strength of the link (correlations between 0.3-0.7), and the maximum lag (3 to 10 years).

We have shown that, in coupled climate models at least, subsurface density anomalies in the wstern SPNA are an important predictor of the wider North Atlantic ocean circulation and upper ocean temperature in the SPNA. This importance on the ocean circulation is especially clear at the latitudes of the SPNA itself. Given the important role of the wind in driving lower latitude AMOC anomalies, and the range of processes by which wind can act on the AMOC (Duchez et al., 2014b, 2014a; Kanzow et al., 2010; Polo et al., 2014; Zhao and Johns, 2014) it is not surprising that the relationship between LSD and AMOC at 26°N is much weaker. Nevertheless, the reasons behind the large spread in these relationships across models is not so clear.

We have tried to constrain this uncertainty by looking at a range of observed metrics that may explain the spread in the correlation strength, including the density anomalies on the western boundary, the stratification of the Labrador Sea, and the mean-AMOC strength. Overall, these constraints point to a relatively weak relationship between LSD and AMOC at 26°N on decadal timescales (i.e. r ~ 0.4) in the real world. However, there are many reasons why this number is still very uncertain. The simulations and observation-based datasets are not directly comparable, as they differ in the background radiative forcing levels, the length of the period used to compute the climatologies, and even the way some indices, like the AMOC, are computed. There is also emerging evidence that models underestimate AMOC variability on decadal timescales (Roberts et al., 2013; Yan et al., 2018). We also recognise that there is large uncertainty within the observationally derived metrics. For example, the assimilation run in DePreSys3, which is used to constrain relationships clearly does not represent the mean AMOC strength at 26°N from RAPID (see Figure 8b). Models generally tend to underestimate the depth of the return flow, and this may still affect how density anomalies project on the basin-wide AMOC. It has also been argued that ocean-only models produce too much deep water in the western basin and Labrador Sea (i.e., Li et al., 2019), and recent observations even challenge the prevailing view from models that Labrador Sea convection dominates the AMOC variability (Koenigk and Brodeau, 2017), suggesting that the key deep water formation occurs North East of the Labrador Sea (Lozier et al., 2019). Therefore, further in-depth study is required to understand the uncertainty in the relationships.

Most of the models considered in this study have relatively coarse resolution, including non-eddying oceans (≥ 1°x1°), which means that they might be missing some key dynamics for the AMOC (Johnson et al., 2019) that could be important to represent realistic linkages. The current analysis, however, includes two models at eddy-permitting resolution (HadGEM3-GC2 and HiGEM), whose relationships lie within the spread of those in the coarser models, suggesting that climatological features (like Labrador Sea stratification) can be more important than the representation of mesoscale processes. However, it could be that higher resolution is needed (e.g. enabling meso-scale eddies in subpolar latitudes) to identify substantial

differences (Hirschi et al., 2020; Johnson et al., 2019). A recent analysis based on HadGEM3-GC3.1 (a later version of
510   HadGEM3-GC2) configured at different horizontal resolutions has shown that long-standing model biases, including in the
North Atlantic, are reduced at eddy-resolving resolution (1/12° x 1/12° in the ocean), and that the strength of the AMOC, the
boundary currents and the northward heat transport is higher than for the coarser resolutions (Hirschi et al., 2020; Roberts et
al., 2019). High resolution coupled models also generally support the new view from OSNAP observations in which the
largest fraction of AMOC variability (on sub annual to decadal timescales) originates at the eastern SPNA (Hirschi et al.,
515   2020). Eddy-resolving resolutions have also been shown in a multi-model study (Roberts et al., 2020) to represent the AMOC
response at 26°N differently in future projections, leading to stronger declines than in non-eddying simulations, declines
mostly associated with a weakening in the Florida Current. Roberts et al. (2020) also compares the meridional coherence of
the AMOC, which does not seem to be resolution-dependent, a result that is in line with another multi-model comparison
between non-eddying and eddy-permitting simulations (Li et al., 2019).

520   Despite the current limitations in the models considered for this study, it is important to highlight that they provide a rather
consistent picture of a chain of relationships in the North Atlantic that is able to explain some of the recent observed trends
(Robson et al. 2016). This paper has broadly characterized this behaviour, and highlighted the uncertainty. These relationships
are also consistent with the mechanisms proposed by Yeager and Robson (2017) to explain high levels of predictive skill in
the SPNA on decadal timescales. Our analysis has also helped to identify specific metrics (such as LSD stratification and the
525   depth of the boundary density) that could be used as emergent constraints for future projections, i.e. to subset the simulations
expected to more realistically represent the future changes in the region. Having a more realistic subpolar gyre stratification at
present day conditions has been shown in CMIP5 simulations to increase the probability of a future collapse in convection
(Sgubin et al., 2017), that would lead to a widespread SPG cooling. It remains to be tested if similar conclusions can be drawn
from eddy-resolving simulations.

530

Code availability. The main scripts used in the analysis and other supporting information that may be useful to reproduce the
results of this article are archived at the Barcelona Supercomputing Center and will be shared upon request by the
corresponding author.

Data availability. Outputs from the CMIP5 simulations can be downloaded from the corresponding ESGF node: https://esgf-
535   node.llnl.gov/projects/cmip5/. EN4 observations used in this study correspond to version 2.1 of the dataset, available at
https://www.metoffice.gov.uk/hadobs/en4/download-en4-2-1.html. Outputs from the GC2, HiGEM and DePreSys simulations
are available upon request to the corresponding author.

Author contributions. P. O., J. R. and R. S. conceived the study, which was later discussed and refined with the other co-
authors. M. M. downloaded and processed the CMIP5 data, computing the main climate indices. P. O. led the analysis, and
540   together with J. R. prepared the manuscript with contributions from all co-authors.

Competing interests. The authors declare that they have no conflict of interest.

Acknowledgements. We thank the UK Met Office for providing the model data of GC2 used in this study, and all the
research centers that contributed to CMIP5 and made their data available. This work was largely funded by the NERC Project

"Dynamics and Predictability of the Atlantic Meridional Overturning and Climate Project" (DYNAMOC, NE/ M005127/1). P.
545 O. work was additionally supported by the Spanish Ministry of Economy, Industry and Competitivity through the Ramon y
Cajal grant RYC-2017-22772. J. R. was additionally supported by the NERC ACSIS program and R. S. by NERC via the
National Centre for Atmospheric Science (NCAS).

550 **References**

Baehr, J., Hirschi, J., Beismann, J.-O. and Marotzke, J.: Monitoring the meridional overturning circulation in the North
Atlantic: A model-based array design study, J. Mar. Res., 62(3), 283–312, doi:10.1357/0022240041446191, 2004.

Barrier, N., Cassou, C., Deshayes, J. and Treguier, A.-M.: Response of North Atlantic Ocean Circulation to Atmospheric
Weather Regimes, J. Phys. Oceanogr., 44(1), 179–201, doi:10.1175/JPO-D-12-0217.1, 2014.

555 Bingham, R. J. and Hughes, C. W.: Geostrophic dynamics of meridional transport variability in the subpolar North Atlantic, J.
Geophys. Res. Oceans, 114(C12), doi:10.1029/2009JC005492, 2009.

Bretherton, C. S., Widmann, M., Dymnikov, V. P., Wallace, J. M. and Blad??, I.: The effective number of spatial degrees of
freedom of a time-varying field, J. Clim., 12(7), 1990–2009, doi:10.1175/1520-0442(1999)012<1990:TENOSD>2.0.CO;2,
1999.

560 Bryan, K.: Climate and the Ocean Circulation: III. The Ocean Model, Mon. Weather Rev., 97(11), 806–827,
doi:10.1175/1520-0493(1969)097<0806:CATOC>2.3.CO;2, 1969.

Caesar, L., Rahmstorf, S., Robinson, A., Feulner, G. and Saba, V.: Observed fingerprint of a weakening Atlantic Ocean
overturning circulation, Nature, 556(7700), 191–196, doi:10.1038/s41586-018-0006-5, 2018.

Danabasoglu, G.: On multidecadal variability of the Atlantic meridional overturning circulation in the community climate
565 system model version 3, J. Clim., 21, 5524–5544, doi:10.1175/2008JCLI2019.1, 2008.

Desbruyères, D. G., Mercier, H., Maze, G. and Daniault, N.: Surface predictor of overturning circulation and heat content
change in the subpolar North Atlantic, Ocean Sci, 15(3), 809–817, doi:10.5194/os-15-809-2019, 2019.

Dong, B. and Sutton, R. T.: Mechanism of interdecadal thermohaline circulation variability in a coupled ocean-atmosphere
GCM, J. Clim., 18(1964), 1117–1135, doi:10.1175/JCLI3328.1, 2005.

570 Duchez, A., Hirschi, J. J.-M., Cunningham, S. A., Blaker, A. T., Bryden, H. L., de Cuevas, B., Atkinson, C. P., McCarthy, G.
D., Frajka-Williams, E., Rayner, D., Smeed, D. and Mizielinski, M. S.: A New Index for the Atlantic Meridional Overturning
Circulation at 26°N, J. Clim., 27(17), 6439–6455, doi:10.1175/JCLI-D-13-00052.1, 2014a.

Duchez, A., Frajka-Williams, E., Castro, N., Hirschi, J. and Coward, A.: Seasonal to interannual variability in density around
the Canary Islands and their influence on the Atlantic meridional overturning circulation at 26°N, J. Geophys. Res. Oceans,
575 119(3), 1843–1860, doi:10.1002/2013JC009416, 2014b.

Duchez, A., Frajka-Williams, E., Josey, S. A., Evans, D. G., Grist, J. P., Marsh, R., McCarthy, G. D., Sinha, B., Berry, D. I.
and Hirschi, J. J.-M.: Drivers of exceptionally cold North Atlantic Ocean temperatures and their link to the 2015 European
heat wave, Environ. Res. Lett., 11(7), 074004, doi:10.1088/1748-9326/11/7/074004, 2016.

Dunstone, N., Smith, D., Scaife, A., Hermanson, L., Eade, R., Robinson, N., Andrews, M. and Knight, J.: Skilful predictions
580 of the winter North Atlantic Oscillation one year ahead, Nat. Geosci., 9, 809, 2016.

Flato, G., Marotzke, J., Abiodun, B., Braconnot, P., Chou, S. C., Collins, W., Cox, P., Driouech, F., Emori, S., Eyring, V.,
Forest, C., Gleckler, P., Guilyardi, E., Jakob, C., Kattsov, V., Reason, C. and Rummukainen, M.: IPCC 2013 AR5 - Chapter 9:
Evaluation of Climate Models, Clim. Change 2013 Phys. Sci. Basis Contrib. Work. Group Fifth Assess. Rep. Intergov. Panel
Clim. Change, doi:10.1017/CBO9781107415324, 2013.

585 Good, S. A., Martin, M. J. and Rayner, N. A.: EN4: quality controlled ocean temperature and salinity profiles and monthly
objective analyses with uncertainty estimates, J Geophys Res, 118, 6704–6716, 2013.

Grist, J. P., Josey, S. a., Marsh, R., Kwon, Y. O., Bingham, R. J. and Blaker, A. T.: The surface-forced overturning of the
North Atlantic: Estimates from modern era atmospheric reanalysis datasets, J. Clim., 27, 3596–3618, doi:10.1175/JCLI-D-13-
00070.1, 2014.

590 Häkkinen, S. and Rhines, P. B.: Decline of subpolar North Atlantic circulation during the 1990s., Science, 304(2004), 555–
559, doi:10.1126/science.1094917, 2004.

Hermanson, L., Eade, R., Robinson, N. H., Dunstone, N. J., Andrews, M. B., Knight, J. R., Scaife, A. A. and Smith, D. M.: Forecast cooling of the Atlantic subpolar gyre and associated impacts, Geophys. Res. Lett., 41(14), 5167–5174, doi:10.1002/2014GL060420, 2014.

595   Hirschi, J. J.-M., Barnier, B., Böning, C., Biastoch, A., Blaker, A. T., Coward, A., Danilov, S., Drijfhout, S., Getzlaff, K., Griffies, S. M., Hasumi, H., Hewitt, H., Iovino, D., Kawasaki, T., Kiss, A. E., Koldunov, N., Marzocchi, A., Mecking, J. V., Moat, B., Molines, J.-M., Myers, P. G., Penduff, T., Roberts, M., Treguier, A.-M., Sein, D. V., Sidorenko, D., Small, J., Spence, P., Thompson, L., Weijer, W. and Xu, X.: The Atlantic meridional overturning circulation in high resolution models, J. Geophys. Res. Oceans, n/a(n/a), e2019JC015522, doi:10.1029/2019JC015522, 2020.

600   Hodson, D. L. R. and Sutton, R. T.: The impact of resolution on the adjustment and decadal variability of the Atlantic meridional overturning circulation in a coupled climate model, Clim. Dyn., 39(12), 3057–3073, doi:10.1007/s00382-012-1309-0, 2012.

Holliday, N. P., Bersch, M., Berx, B., Chafik, L., Cunningham, S., Florindo-López, C., Hátún, H., Johns, W., Josey, S. A., Larsen, K. M. H., Mulet, S., Oltmanns, M., Reverdin, G., Rossby, T., Thierry, V., Valdimarsson, H. and Yashayaev, I.: Ocean
605   circulation causes the largest freshening event for 120 years in eastern subpolar North Atlantic, Nat. Commun., 11(1), 585, doi:10.1038/s41467-020-14474-y, 2020.

Jackson, L. C., Peterson, K. A., Roberts, C. D. and Wood, R. A.: Recent slowing of Atlantic overturning circulation as a recovery from earlier strengthening, Nat. Geosci, 9(7), 518–522, 2016.

Jackson, L. C., Dubois, C., Forget, G., Haines, K., Harrison, M., Iovino, D., Köhl, A., Mignac, D., Masina, S., Peterson, K. A.,
610   Piecuch, C. G., Roberts, C. D., Robson, J., Storto, A., Toyoda, T., Valdivieso, M., Wilson, C., Wang, Y. and Zuo, H.: The Mean State and Variability of the North Atlantic Circulation: A Perspective From Ocean Reanalyses, J. Geophys. Res. Oceans, 124(12), 9141–9170, doi:10.1029/2019JC015210, 2019.

Johnson, H. L., Cessi, P., Marshall, D. P., Schloesser, F. and Spall, M. A.: Recent Contributions of Theory to Our Understanding of the Atlantic Meridional Overturning Circulation, J. Geophys. Res. Oceans, 124(8), 5376–5399,
615   doi:10.1029/2019JC015330, 2019.

Josey, S. A., Hirschi, J. J.-M., Sinha, B., Duchez, A., Grist, J. P. and Marsh, R.: The Recent Atlantic Cold Anomaly: Causes, Consequences, and Related Phenomena, Annu. Rev. Mar. Sci., 10(1), 475–501, doi:10.1146/annurev-marine-121916-063102, 2018.

Jungclaus, J. H., Haak, H., Latif, M. and Mikolajewicz, U.: Arctic-North Atlantic interactions and multidecadal variability of
620   the meridional overturning circulation, J. Clim., 18(19), 4013–4031, doi:10.1175/JCLI3462.1, 2005.

Kanzow, T., Cunningham, S. A., Johns, W. E., Hirschi, J. J.-M., Marotzke, J., Baringer, M. O., Meinen, C. S., Chidichimo, M. P., Atkinson, C., Beal, L. M., Bryden, H. L. and Collins, J.: Seasonal Variability of the Atlantic Meridional Overturning Circulation at 26.5°N, J. Clim., 23(21), 5678–5698, doi:10.1175/2010JCLI3389.1, 2010.

Karspeck, A. R., Stammer, D., Köhl, A., Danabasoglu, G., Balmaseda, M., Smith, D. M., Fujii, Y., Zhang, S., Giese, B.,
625   Tsujino, H. and Rosati, A.: Comparison of the Atlantic meridional overturning circulation between 1960 and 2007 in six ocean reanalysis products, Clim. Dyn., Published Online-Published Online, doi:10.1007/s00382-015-2787-7, 2015.

Katsman, C. A., Drijfhout, S. S., Dijkstra, H. A. and Spall, M. A.: Sinking of Dense North Atlantic Waters in a Global Ocean Model: Location and Controls, J. Geophys. Res. Oceans, 123(5), 3563–3576, doi:10.1029/2017JC013329, 2018.

Kim, W. M., Yeager, S. and Danabasoglu, G.: Atlantic Multidecadal Variability and Associated Climate Impacts Initiated by
630   Ocean Thermohaline Dynamics, J. Clim., 33(4), 1317–1334, doi:10.1175/JCLI-D-19-0530.1, 2019.

Knight, J. R., Allan, R. J., Folland, C. K., Vellinga, M. and Mann, M. E.: A signature of persistent natural thermohaline circulation cycles in observed climate, Geophys. Res. Lett., 32, 1–4, doi:10.1029/2005GL024233, 2005.

Knight, J. R., Folland, C. K. and Scaife, A. a.: Climate impacts of the Atlantic multidecadal oscillation, Geophys. Res. Lett., 33, 1–4, doi:10.1029/2006GL026242, 2006.

635   Koenigk, T. and Brodeau, L.: Arctic climate and its interaction with lower latitudes under different levels of anthropogenic warming in a global coupled climate model, Clim. Dyn., 49(1), 471–492, doi:10.1007/s00382-016-3354-6, 2017.

Langehaug, H. R., Rhines, P. B., Eldevik, T., Mignot, J. and Lohmann, K.: Water mass transformation and the North Atlantic Current in three multicentury climate model simulations, J. Geophys. Res. Oceans, 117(C11), doi:10.1029/2012JC008021, 2012.

640   Li, F., Lozier, M. S., Danabasoglu, G., Holliday, N. P., Kwon, Y.-O., Romanou, A., Yeager, S. G. and Zhang, R.: Local and Downstream Relationships between Labrador Sea Water Volume and North Atlantic Meridional Overturning Circulation Variability, J. Clim., 32(13), 3883–3898, doi:10.1175/JCLI-D-18-0735.1, 2019.

Lohmann, K., Drange, H. and Bentsen, M.: Response of the North Atlantic subpolar gyre to persistent North Atlantic oscillation like forcing, Clim. Dyn., 32, 273–285, doi:10.1007/s00382-008-0467-6, 2009.

645 Lozier, M. S., Leadbetter, S., Williams, R. G., Roussenov, V., Reed, M. S. C. and Moore, N. J.: The spatial pattern and mechanisms of heat-content change in the North Atlantic., Science, 319, 800–803, doi:10.1126/science.1146436, 2008.

Lozier, M. S., Li, F., Bacon, S., Bahr, F., Bower, A. S., Cunningham, S. A., de Jong, M. F., de Steur, L., deYoung, B., Fischer, J., Gary, S. F., Greenan, B. J. W., Holliday, N. P., Houk, A., Houpert, L., Inall, M. E., Johns, W. E., Johnson, H. L., Johnson, C., Karstensen, J., Koman, G., Le Bras, I. A., Lin, X., Mackay, N., Marshall, D. P., Mercier, H., Oltmanns, M., Pickart, R. S.,

650 Ramsey, A. L., Rayner, D., Straneo, F., Thierry, V., Torres, D. J., Williams, R. G., Wilson, C., Yang, J., Yashayaev, I. and Zhao, J.: A sea change in our view of overturning in the subpolar North Atlantic, Science, 363(6426), 516, doi:10.1126/science.aau6592, 2019.

McCarthy, G. D., Haigh, I. D., Hirschi, J. J.-M., Grist, J. P. and Smeed, D. A.: Ocean impact on decadal Atlantic climate variability revealed by sea-level observations., Nature, 521(7553), 508–510, doi:10.1038/nature14491, 2015.

655 Menary, M. B., Hodson, D. L. R., Robson, J. I., Sutton, R. T., Wood, R. A. and Hunt, J. A.: Exploring the impact of CMIP5 model biases on the simulation of North Atlantic decadal variability, Geophys. Res. Lett., 42(14), 5926–5934, doi:10.1002/2015GL064360, 2015.

Moat, B. I., Sinha, B., Josey, S. A., Robson, J., Ortega, P., Sévellec, F., Holliday, N. P., McCarthy, G. D., New, A. L. and Hirschi, J. J.-M.: Insights into Decadal North Atlantic Sea Surface Temperature and Ocean Heat Content Variability from an

660 Eddy-Permitting Coupled Climate Model, J. Clim., 32(18), 6137–6161, doi:10.1175/JCLI-D-18-0709.1, 2019.

Monerie, P.-A., Robson, J., Dong, B., Dieppois, B., Pohl, B. and Dunstone, N.: Predicting the seasonal evolution of southern African summer precipitation in the DePreSys3 prediction system, Clim. Dyn., 52(11), 6491–6510, doi:10.1007/s00382-018-4526-3, 2019.

Ortega, P., Hawkins, E. and Sutton, R.: Processes governing the predictability of the Atlantic meridional overturning

665 circulation in a coupled GCM, Clim. Dyn., 37(9–10), doi:10.1007/s00382-011-1025-1, 2011.

Ortega, P., Mignot, J., Swingedouw, D., Sévellec, F. and Guilyardi, E.: Reconciling two alternative mechanisms behind bi-decadal variability in the North Atlantic, Prog. Oceanogr., 137, doi:10.1016/j.pocean.2015.06.009, 2015.

Ortega, P., Robson, J., Sutton, R. T. and Andrews, M. B.: Mechanisms of decadal variability in the Labrador Sea and the wider North Atlantic in a high-resolution climate model, Clim. Dyn., 49(7–8), doi:10.1007/s00382-016-3467-y, 2017.

670 Pickart, R. S. and Spall, M. a.: Impact of Labrador Sea Convection on the North Atlantic Meridional Overturning Circulation, J. Phys. Oceanogr., 37(1993), 2207–2227, doi:10.1175/JPO3178.1, 2007.

Piecuch, C. G., Ponte, R. M., Little, C. M., Buckley, M. W. and Fukumori, I.: Mechanisms underlying recent decadal changes in subpolar North Atlantic Ocean heat content, J. Geophys. Res. Oceans, 122(9), 7181–7197, doi:10.1002/2017JC012845, 2017.

675 Polo, I., Robson, J., Sutton, R. and Balmaseda, M. A.: The Importance of Wind and Buoyancy Forcing for the Boundary Density Variations and the Geostrophic Component of the AMOC at 26°N, J. Phys. Oceanogr., 44(9), 2387–2408, doi:10.1175/JPO-D-13-0264.1, 2014.

Rahmstorf, S., Box, J. E., Feulner, G., Mann, M. E., Robinson, A., Rutherford, S. and Schaffernicht, E. J.: Exceptional twentieth-century slowdown in Atlantic Ocean overturning circulation, Nat. Clim. Change, 5(5), 475–480,

680 doi:10.1038/nclimate2554, 2015.

Reintges, A., Martin, T., Latif, M. and Keenlyside, N. S.: Uncertainty in twenty-first century projections of the Atlantic Meridional Overturning Circulation in CMIP3 and CMIP5 models, Clim. Dyn., 49(5), 1495–1511, doi:10.1007/s00382-016-3180-x, 2017.

Reverdin, G.: North Atlantic subpolar Gyre surface variability (1895-2009), J. Clim., 23, 4571–4584,

685 doi:10.1175/2010JCLI3493.1, 2010.

Roberts, C. D., Garry, F. K. and Jackson, L. C.: A Multimodel Study of Sea Surface Temperature and Subsurface Density Fingerprints of the Atlantic Meridional Overturning Circulation, J. Clim., 26(22), 9155–9174, doi:10.1175/JCLI-D-12-00762.1, 2013.

Roberts, M. J., Baker, A., Blockley, E. W., Calvert, D., Coward, A., Hewitt, H. T., Jackson, L. C., Kuhlbrodt, T., Mathiot, P.,

690 Roberts, C. D., Schiemann, R., Seddon, J., Vannière, B. and Vidale, P. L.: Description of the resolution hierarchy of the global coupled HadGEM3-GC3.1 model as used in CMIP6 HighResMIP experiments, Geosci Model Dev, 12(12), 4999–5028, doi:10.5194/gmd-12-4999-2019, 2019.

Roberts, M. J., Jackson, L. C., Roberts, C. D., Meccia, V., Docquier, D., Koenigk, T., Ortega, P., Moreno-Chamarro, E.,

695 Bellucci, A., Coward, A., Drijfhout, S., Exarchou, E., Gutjahr, O., Hewitt, H. T., Iovino, D., Lohmann, K., Schiemann, R., Seddon, J., Terray, L., Xu, X., Zhang, Q., Chang, P., Yeager, S. G., Castruccio, F., Zhang, S. and Wu, L.: Sensitivity of the Atlantic Meridional Overturning Circulation to Model Resolution in CMIP6 HighResMIP Simulations and Implications for Future Changes, JAMES, Published online, 2020.

Robson, J., Lohmann, K., Smith, D. and Palmer, M. D.: Causes of the rapid warming of the North Atlantic Ocean in the mid-1990s, J. Clim., 25(2008), 4116–4134, doi:10.1175/JCLI-D-11-00443.1, 2012.

700 Robson, J., Sutton, R. and Smith, D.: Predictable climate impacts of the decadal changes in the ocean in the 1990s, J. Clim., 26, 6329–6339, doi:10.1175/JCLI-D-12-00827.1, 2013.

Robson, J., Hodson, D., Hawkins, E. and Sutton, R.: Atlantic overturning in decline?, Nat. Geosci., 7(1), 2–3, doi:10.1038/ngeo2050, 2014.

Robson, J., Ortega, P. and Sutton, R.: A reversal of climatic trends in the North Atlantic since 2005, Nat. Geosci., 9(7),
705 doi:10.1038/ngeo2727, 2016.

Robson, J., Polo, I., Hodson, D. L. R., Stevens, D. P. and Shaffrey, L. C.: Decadal prediction of the North Atlantic subpolar gyre in the HiGEM high-resolution climate model, Clim. Dyn., 50(3), 921–937, doi:10.1007/s00382-017-3649-2, 2018a.

Robson, J., Sutton, R. T., Archibald, A., Cooper, F., Christensen, M., Gray, L. J., Holliday, N. P., Macintosh, C., McMillan, M., Moat, B., Russo, M., Tilling, R., Carslaw, K., Desbruyères, D., Embury, O., Feltham, D. L., Grosvenor, D. P., Josey, S.,
710 King, B., Lewis, A., McCarthy, G. D., Merchant, C., New, A. L., O'Reilly, C. H., Osprey, S. M., Read, K., Scaife, A., Shepherd, A., Sinha, B., Smeed, D., Smith, D., Ridout, A., Woollings, T. and Yang, M.: Recent multivariate changes in the North Atlantic climate system, with a focus on 2005–2016, Int. J. Climatol., 38(14), 5050–5076, doi:10.1002/joc.5815, 2018b.

Roussenov, V. M., Williams, R. G., Hughes, C. W. and Bingham, R. J.: Boundary wave communication of bottom pressure and overturning changes for the North Atlantic, J. Geophys. Res. Oceans, 113(C8), doi:10.1029/2007JC004501, 2008.

715 Schlesinger, M. E. and Ramankutty, N.: An oscillation in the global climate system of period 65-70 years, Nature, 367(6465), 723–726, 1994.

Sgubin, G., Swingedouw, D., Drijfhout, S., Mary, Y. and Bennabi, A.: Abrupt cooling over the North Atlantic in modern climate models, Nat. Commun., 8 [online] Available from: http://dx.doi.org/10.1038/ncomms14375, 2017.

Shaffrey, L., Stevens, I., Norton, W. A., Roberts, M. J., Vidale, P. L., Harle, J. D., Jrrar, A., Stevens, D. P., Woodage, M. J.,
720 Demory, M. E., Donners, J., Clark, D. B., Clayton, A., Cole, J. W., Wilson, S. S., Connolley, W. M., Davi, T. M. and Martin, G. M.: U.K. HiGEM: The New U.K. High-Resolution Global Environment Model—Model Description and Basic Evaluation, J. Clim., 22(8), 1861–1896, doi:10.1175/2008JCLI2508.1, 2009.

Sinha, B., Smeed, D. A., McCarthy, G., Moat, B. I., Josey, S. A., Hirschi, J. J.-M., Frajka-Williams, E., Blaker, A. T., Rayner, D. and Madec, G.: The accuracy of estimates of the overturning circulation from basin-wide mooring arrays, Prog. Oceanogr.,
725 160, 101–123, doi:10.1016/j.pocean.2017.12.001, 2018.

Smeed, D. A., Josey, S. A., Beaulieu, C., Johns, W. E., Moat, B. I., Frajka-Williams, E., Rayner, D., Meinen, C. S., Baringer, M. O., Bryden, H. L. and McCarthy, G. D.: The North Atlantic Ocean Is in a State of Reduced Overturning, Geophys. Res. Lett., 45(3), 1527–1533, doi:10.1002/2017GL076350, 2018.

Smith, D. M. and Murphy, J. M.: An objective ocean temperature and salinity analysis using covariances from a global climate
730 model, J. Geophys. Res. Oceans, 112(C2), doi:10.1029/2005JC003172, 2007.

Sutton, R. T. and Hodson, D. L. R.: Atlantic Ocean forcing of North American and European summer climate., Science, 309(2005), 115–118, doi:10.1126/science.1109496, 2005.

Sutton, R. T., McCarthy, G. D., Robson, J., Sinha, B., Archibald, A. T. and Gray, L. J.: Atlantic Multidecadal Variability and the U.K. ACSIS Program, Bull. Am. Meteorol. Soc., 99(2), 415–425, doi:10.1175/BAMS-D-16-0266.1, 2018.

735 Taylor, K. E., Stouffer, R. J. and Meehl, G. A.: An Overview of CMIP5 and the Experiment Design, Bull. Am. Meteorol. Soc., 93(4), 485–498, doi:10.1175/BAMS-D-11-00094.1, 2012.

Thornalley, D. J. R., Oppo, D. W., Ortega, P., Robson, J. I., Brierley, C. M., Davis, R., Hall, I. R., Moffa-Sanchez, P., Rose, N. L., Spooner, P. T., Yashayaev, I. and Keigwin, L. D.: Anomalously weak Labrador Sea convection and Atlantic overturning during the past 150 years, Nature, 556(7700), doi:10.1038/s41586-018-0007-4, 2018.

740 Weijer, W., Cheng, W., Garuba, O. A., Hu, A. and Nadiga, B. T.: CMIP6 Models Predict Significant 21st Century Decline of the Atlantic Meridional Overturning Circulation, Geophys. Res. Lett., 47(12), e2019GL086075, doi:10.1029/2019GL086075, 2020.

Woollings, T., Gregory, J., Pinto, J. G., Reyers, M. and Brayshaw, D.: Response of the North Atlantic storm track to climate change shaped by ocean–atmosphere coupling, Nat. Geosci., 5(5), 313–317, doi:10.1038/ngeo1438, 2012.

745   Xu, X., Chassignet, E. P. and Wang, F.: On the variability of the Atlantic meridional overturning circulation transports in coupled CMIP5 simulations, Clim. Dyn., 52(11), 6511–6531, doi:10.1007/s00382-018-4529-0, 2019.

Yan, X., Zhang, R. and Knutson, T. R.: Underestimated AMOC Variability and Implications for AMV and Predictability in CMIP Models, Geophys. Res. Lett., 45(9), 4319–4328, doi:10.1029/2018GL077378, 2018.

Yashayaev, I. and Loder, J. W.: Recurrent replenishment of Labrador Sea Water and associated decadal-scale variability, J.

750   Geophys. Res. Oceans, 121, 8095–8114, doi:10.1002/2016JC012046, 2016.

Yeager, S.: Topographic Coupling of the Atlantic Overturning and Gyre Circulations, J. Phys. Oceanogr., 45(5), 1258–1284, doi:10.1175/JPO-D-14-0100.1, 2015.

Yeager, S. and Danabasoglu, G.: The Origins of Late-Twentieth-Century Variations in the Large-Scale North Atlantic Circulation, J. Clim., 27(9), 3222–3247, doi:10.1175/JCLI-D-13-00125.1, 2014.

755   Yeager, S. G. and Robson, J. I.: Recent Progress in Understanding and Predicting Atlantic Decadal Climate Variability, Curr. Clim. Change Rep., 3(2), 112–127, doi:10.1007/s40641-017-0064-z, 2017.

Zhang, L. and Wang, C.: Multidecadal North Atlantic sea surface temperature and Atlantic meridional overturning circulation variability in CMIP5 historical simulations, J. Geophys. Res. Oceans, 118(10), 5772–5791, doi:10.1002/jgrc.20390, 2013.

Zhang, R.: Coherent surface-subsurface fingerprint of the Atlantic meridional overturning circulation, Geophys. Res. Lett., 35,

760   1–6, doi:10.1029/2008GL035463, 2008.

Zhang, R. and Delworth, T. L.: Impact of Atlantic multidecadal oscillations on India/Sahel rainfall and Atlantic hurricanes, Geophys. Res. Lett., 33(17), doi:10.1029/2006GL026267, 2006.

Zhang, R., Delworth, T. L., Rosati, A., Anderson, W. G., Dixon, K. W., Lee, H. C. and Zeng, F.: Sensitivity of the North Atlantic Ocean Circulation to an abrupt change in the Nordic Sea overflow in a high resolution global coupled climate model,

765   J. Geophys. Res. Oceans, 116, 1–14, doi:10.1029/2011JC007240, 2011.

Zhao, J. and Johns, W.: Wind-forced interannual variability of the Atlantic Meridional Overturning Circulation at 26.5 N, J. Geophys. Res. Oceans, 2403–2419, doi:10.1002/2013JC009407.Received, 2014.

Zou, S., Lozier, M. S. and Xu, X.: Latitudinal Structure of the Meridional Overturning Circulation Variability on Interannual to Decadal Time Scales in the North Atlantic Ocean, J. Clim., 33(9), 3845–3862, doi:10.1175/JCLI-D-19-0215.1, 2020.

770